Appl Phys A (2013) 113:347–353
DOI 10.1007/s00339-013-7652-0

Applied Physics A
Materials Science & Processing

A high-performance laser energy meter based on anisotropic Seebeck effect in a strongly correlated electronic thin film

G.-Y. Zhang · H.-R. Zheng · W.-H. Huang · X.-Y. Zhang · D.-L. Gao · H. Zhang · P.-X. Zhang · T.-Y. Tseng · H.-U. Habermeier · C.-T. Lin · H.-H. Cheng

Received: 19 December 2012 / Accepted: 27 February 2013 / Published online: 13 March 2013

Abstract We have developed a high-performance laser energy meter based on anisotropic Seebeck effect in a strongly correlated electronic (SCE) thin film. SCE thin films, typically represented by high-temperature superconductor (HTS) cuprate and colossal magnetoresistance (CMR) manganite thin films, demonstrate tremendous anisotropic Seebeck effect. In this study, a $La_{2/3}Ca_{1/3}MnO_3$ thin film grown on a tilted $LaAlO_3$ substrate is tested with the fundamental, the second, the third, and the fourth harmonics (1064, 532, 355, 266 nm, respectively) of a Q-switched Nd:YAG laser over a wide range of temperatures from room temperature to 16 K. The peak-value of the laser-induced thermoelectric voltage signal shows a good linear relationship with the laser energy per pulse in the measured wavelength and temperature ranges. The combined advantages over other commercial laser detectors such as nanosecond-order response and spectrally broad and flat response over a wide range of temperatures, in situ real-time measurement, and energy savings, make the device an ideal candidate for next-generation laser detectors and laser power/energy meters.

G.-Y. Zhang · H.-H. Cheng (✉)
Center for Condensed Matter Science, National Taiwan University, Taipei 106, Taiwan
e-mail: hhcheng@ntu.edu.tw

G.-Y. Zhang · T.-Y. Tseng
Department of Electronics Engineering and Institute of Electronics, National Chiao Tung University, Hsinchu 300, Taiwan

G.-Y. Zhang
Hefei National Laboratory for Physical Science at Microscal, University of Science and Technology of China, Hefei 230026, People's Republic of China

G.-Y. Zhang (✉) · W.-H. Huang
Department of Precision Machinery and Instrumentation, University of Science and Technology of China, Hefei 230026, People's Republic of China
e-mail: zhanggy@ustc.edu.cn

H.-R. Zheng · X.-Y. Zhang · D.-L. Gao
School of Physics and Information Technology, Shaanxi Normal University, Xi'an 710062, People's Republic of China

H. Zhang · P.-X. Zhang
Institute of Advanced Materials for Photoelectronics, Kunming University of Science and Technology, Kunming 650051, People's Republic of China

H.-U. Habermeier · C.-T. Lin
Max Planck Institute for Solid State Research, Heisenbergstrasse 1, 70569 Stuttgart, Germany

1 Introduction

Laser-induced thermoelectric voltage effect (LITV) in strongly correlated electronic (SCE) thin films has attracted much attention since it was discovered in high-temperature superconductor (HTS) cuprate [$YBaCuO_{7-\sigma}$ (YBCO) and $Bi_2Sr_2CaCu_2O_8$ (BSCCO)] thin films grown on tilted single-crystal substrates at the beginning of 1990 [1], which is not only due to its importance in exploring new physics but also due to the great application potential for developing new radiation detectors to improve the optical measuring systems, e.g., the near optical system [2–5].

The LITV effect has been proved to be an anisotropic Seebeck effect in HTS cuprate thin films [6]. It is known that the Seebeck coefficient of a pure metal or an alloy is a scalar; however, the Seebeck coefficient of a single crystal is usually a tensor [7, 8]. In case of HTS cuprate thin films, the Seebeck coefficient of the CuO_2 layer is different

from that along the c-axis, which can be denoted by S_{ab} and S_c, respectively. When an epitaxial thin film is grown on a tilted single crystal, its c-axis inclines an angle to the normal of its surface, and the sequence of the conducting CuO_2 layers and the less-conducting intermediate layers forms an atomic layer thermopile (ALT) that consists of some millions of atomic scale thermocouples [9]. When the upper part of the film is irradiated by a laser pulse, its temperature raises, and a temperature gradient erects in the inner of the thin film, and, as a result, a voltage signal generates across the thin film due to the ALT effect, that is, the microscopic scene of the LITV effect [10].

Colossal magnetoresistance (CMR) manganite thin films of the general formula $Ln_{1-x}A_xMnO_3$ (with Ln = rare-earth ion and A = alkaline-earth ion) are other attractive SCE systems which have versatile electronic, optical, magnetic, and structural properties [11]. Doping plays an important role in determining the electrical and magnetic properties. For the $La_{1-x}Ca_xMnO_3$ (LCMO) materials, the phase diagram shows that in the doping range $0.2 < x < 0.5$, they are ferromagnetic and metallic; at $x = 0.5$, they can be ferromagnetic and charge-ordered antiferromagnetic at ~220 and ~150 K, respectively; while in the range $0.5 < x < 0.9$, they can be antiferromagnetic and charge ordered [5]. Typically, $La_{2/3}Ca_{1/3}MnO_3$ thin films demonstrate CMR effect, metal–insulator transition, and colossal pressure-induced negative resistance change, which find promising applications in developing magnetic sensors, bolometers, and pressure sensors [11, 12]. It is unexpected that a large LITV effect can be observed in $La_{2/3}Ca_{1/3}MnO_3$ thin films grown on tilted $SrTiO_3$ single-crystal substrates [13, 14]; because LCMO has a quasi-cubic structure, it seems that no large anisotropy could be generated compared with the layered structures of HTS materials. However, the characteristics of the LITV signals in CMR thin films are in remarkable analogy to the results reported for HTS thin films, which reveal an identical physical origin in both materials, the anisotropic Seebeck effect. In view of the fact that the doping level x influences the magnitude of a LITV signal greatly, it is inferred that the large anisotropy results from the long-range cooperative Jahn–Teller distortions caused by the Mn^{3+} ions [14].

Temperature is a very important factor influencing on the detector performance. It was reported that the LITV signals of the YBCO thin films response to an Nd:YAG laser ($\lambda = 532$ nm) could be recorded from 300 K to above T_c (typically 89 K), but they disappeared below T_c [15]; while in LCMO thin films the LITV signals could be measured in the temperature range from 300 to 20 K using a KrF excimer laser ($\lambda = 248$ nm, pulse duration 28 ns) [13]. The results show that LCMO thin films have better low-temperature performance than YBCO thin films, indicating a great potential for laser detector applications. Based on SCE, pyroelectric, and piezoelectric materials peak-voltage-type laser energy/power meters have been developed; however, they operate at room temperature (RT), and the studies on low-temperature devices are lacking [16–22]. It is known that low-temperature detectors (LTDs), including transition edge sensors (TESs), superconducting tunnel junctions (STJs), superconducting stripline detectors (SSDs), bolometers, single-photon detectors, etc., are widely used in cosmology, astronomy, particle physics, nuclear physics, dark matter searches, terahertz research, infrared technology, X-ray spectroscopy, surface analysis, large molecules mass spectrometry, nuclear nonproliferation, security, quantum computing, quantum teleportation, etc., owing to their advantages over other conventional detectors, such as better energy resolution, lower-energy thresholds, and wider material choice [23–39]. Therefore, it is important for both basic science and applied technology to investigate temperature-dependent properties to develop high-performance LTDs. In our previous study, we designed a time-integral-type SCE $La_{0.8}Sr_{0.2}MnO_3$ thin-film laser energy meter that has the advantages of nanosecond-order response and spectrally broad and flat response at RT [40]. In this work, we developed a peak-voltage-type SCE $La_{2/3}Ca_{1/3}MnO_3$ thin-film laser energy meter that has these advantages not only at RT, but also over a wide range of temperatures from RT to 16 K, which opened new opportunities for SCE detectors for low-temperature applications, e.g., space-based applications (space telescope, satellite communications, laser radar, Mars exploration, Moon landing, etc.). Compared with RT devices, the SCE laser detectors and laser energy meters are energy-saving devices since they can work in low-temperature environment directly without temperature control systems.

2 Theory

The time-dependent open-circuit LITV signal is given by the formula [41]

$$U(t) = \frac{\alpha_0 El \sin(2\alpha)}{4d\rho c_0 \sqrt{\pi Dt}}(S_{ab} - S_c)\left(e^{-\frac{\delta^2}{4Dt}} - e^{-\frac{d^2}{4Dt}}\right), \quad (1)$$

where α_0 is the laser absorption coefficient of film, E is the laser energy density per pulse (for convenience, E also stands for laser energy per pulse), l is the illuminated length of film, α is the tilted angle, $S_{ab} - S_c$ is the Seebeck coefficient anisotropy, ρ is the mass density, c_0 is the specific heat, δ is the laser penetrating depth into the thin film material, D is the thermal diffusion constant, and d is the film thickness.

The peak value of LITV signal U_p is given by the difference or

$$U_p = \frac{\alpha_0 El \sin(2\alpha)}{4\sqrt{\pi} d\rho c_0}(S_{ab} - S_c) f(\delta, d). \quad (2)$$

Letting $U_p = A_p E$, we get

$$A_p = \frac{\alpha_0 l \sin(2\alpha)}{4\sqrt{\pi} d\rho c_0}(S_{ab} - S_c) f(\delta, d), \quad (3)$$

where A_p is the sensitivity, and $f(\delta, d)$ is the function about δ and d. Based on the linear relation $U_p = A_p E$, a peak-voltage-type laser energy meter can be designed. Furthermore, the response time is proportional to $1/D$, while Eq. (3) shows that A_p is independent of D; therefore, we can increase the response speed by increasing D without changing the sensitivity.

3 Experimental

The SCE thin-film samples were prepared by pulsed laser deposition (PLD) method. The bulk targets of LCMO with $x = 0.1 - 0.5$ synthesized by solid-state reaction technique were used for the thin film deposition. A KrF excimer laser ($\lambda = 248$ nm, pulse duration 20 ns, energy density per pulse 200 mJ/cm^2) operated at a repeat rate 3 Hz was used for the LCMO target ablation. All the thin films were deposited onto the polished $LaAlO_3$ single-crystal substrates with $\alpha = 0°$ and 15° at 800 °C in an oxygen atmosphere at a pressure of 50 Pa. After the thin film formation, the samples were annealed at 780 °C in an oxygen atmosphere at a pressure of 100 Pa for 1 h and then slowly cooled down to RT.

In order to investigate the LITV effect in LCMO thin-film devices, Au/Cr electrodes are fabricated on the film surface through thermal evaporation for electrical measurements. The light source is a Q-switched Nd:YAG solid-state laser (pulse duration 10 ns), which has the fundamental, the second, the third, and the fourth harmonics (1064, 532, 355, and 266 nm, respectively) covering a wide range of wavelengths from IR to UV. A cryostat consisting of a liquid He cooling finger and a heater was used to control the sample temperature in the range of 10 K $< T <$ 300 K with an accuracy better than 0.5 K. A commercial laser energy meter was used for measuring the laser output. The LITV signals were recorded by a digital storage oscilloscope, the input impedance (R_i) of which is 50 Ω.

4 Results and discussion

Figure 1 shows a typical θ–2θ XRD spectrum of an LCMO thin film grown on $LaAlO_3$ ($\alpha = 0°$) substrate. Besides the (00l) diffraction peaks, the LCMO thin film shows no other peaks from the impurity phases or randomly oriented gains, indicating that the film is single phase and c-axis preferentially oriented. The rocking curve of the (002) peak has a very small value (0.21°, not shown) of full width at half maximum (FWHM), demonstrating a highly epitaxy and good crystallization of the thin film.

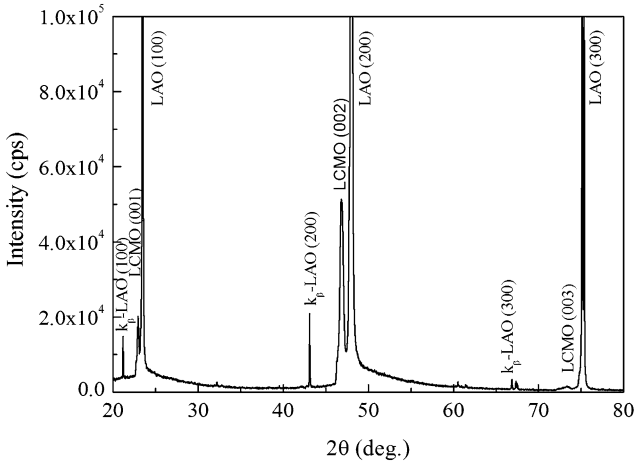

Fig. 1 XRD θ–2θ curve of the LCMO thin film on LAO

The LITV signals of a 250-nm-thick $La_{2/3}Ca_{1/3}MnO_3$ thin film on 15° tilted $LaAlO_3$ substrate to the laser pulses at $\lambda = 1064, 532, 355$, and 266 nm with the repeat rate 10 Hz were measured when the thin film was cooled down from RT (294 K) to 16 K. Figure 2 shows the typical LITV signals. At $T = 294$ K, for $\lambda = 1064, 532, 355$, and 266 nm, response time τ(FWHM) $= 47.0, 43.4, 38.0$, and 65.2 ns, respectively, showing that the $La_{2/3}Ca_{1/3}MnO_3$ thin-film detector has ns-order response over a wide range of wavelengths from IR to UV at RT. In contrast, the HTS thin-film detectors based on LITV effect also demonstrate excellent performance at RT, e.g., in YBCO thin-film detectors LITV signals of ns- and ps-order and response over a more wide range of wavelengths from submillimeter to UV have been measured at RT [10, 42]. Nevertheless, over a wide range of temperatures from RT to 16 K, which is close to the low-temperature limit of the cooling system, tremendous LITV signals of ns-order were observed in the $La_{2/3}Ca_{1/3}MnO_3$ thin-film detector over a wide range of wavelengths from IR to UV. It can be found at $T = 50(16)$ K, for $\lambda = 1064, 532, 355$, and 266 nm, $\tau = 85.2(91.4), 84.2(87.6), 60.8(76.4)$, and 97.2 (103.0) ns, respectively. On the contrary, below T_c (89 K) an YBCO thin-film laser detector shows no LITV effect since the superconducting state occurs. Because most HST materials have a T_c well above 16 K, the $La_{2/3}Ca_{1/3}MnO_3$ thin-film detector has better low-temperature performance than HST thin-film detectors. Furthermore, it can be seen that at each temperature τ varies with wavelength that is attributed to quantum effect. Photon energies for the four laser wavelengths are 1.17 eV (1064 nm), 2.33 eV (532 nm), 3.49 eV (355 nm), and 4.66 eV (266 nm). Except 1064 nm, the other three wavelengths have energies greater than the band gap (1.2 eV) of LCMO and can generate carriers to enhance the conductivity, thereby increasing the response speed. As a result, in the range of wavelengths from 1064

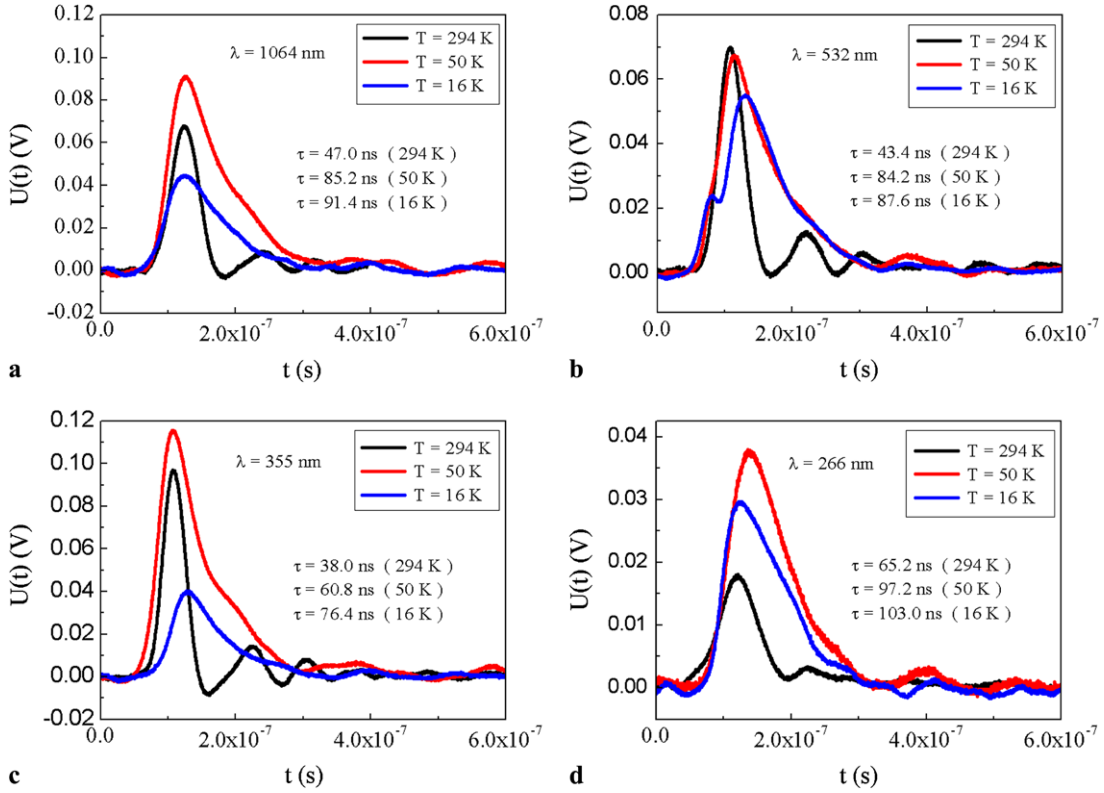

Fig. 2 The LITV signals in the $La_{2/3}Ca_{1/3}MnO_3$ thin film for four wavelengths ($\lambda = 1064, 532, 355, 266$ nm) of a Q-switched Nd:YAG laser at different temperatures ($T = 294, 50, 16$ K)

to 355 nm, τ decreases with wavelength. However, τ has a rise at 266 nm as compared to 355 nm, which can be due to a hot-carrier effect [43, 44]. The laser energy of 266 nm wavelength is so high that it can generate many hot carriers, and a slowing down process is needed before their energies are absorbed by the lattice, and therefore, τ increases. To study temperature-dependent response time of the thin film, the influence of load resistance R_i should be considered. In order to obtain the value of τ_f, which is the FWHM of the LITV signal from thin film, τ, which is the FWHM of the LITV signal from the oscilloscope, should be multiplied by a correcting factor $\eta = (1 + R_f/R_i)$, where R_f is the film resisatance. At $T = 294$, 50, and 16 K, $R_f = 1155.96$, 23.54, and 20.88 Ω, respectively. Substituting the values of R_f, we get $\eta = 24.12$, 1.47, and 1.42, respectively. The dependence of τ_f on wavelength and temperature is shown in Fig. 3. It can be seen that at each temperature, τ_f has spectrally flat response over a wide range of wavelengths from IR to UV, and only in UV region there is a slight variation. At $T = 50(16)$ K, τ_f has a smaller value as compared to RT, which is because at the low temperature the film has a larger thermal diffusion constant [45, 46]. In addition, at $T = 16$ K the cooling system can be disturbed easily by laser energy, and therefore, at $T = 16$ K for each wavelength, τ_f has a greater value than at 50 K.

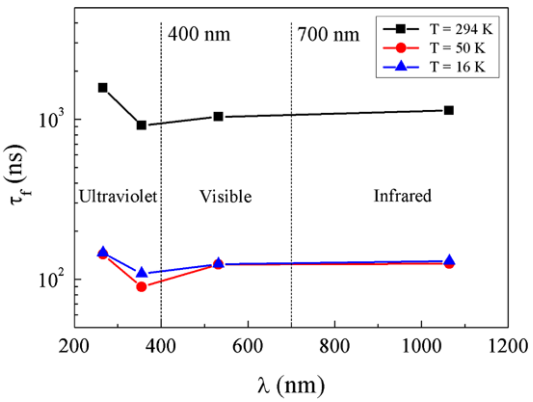

Fig. 3 Wavelength dependence of the response time of the $La_{2/3}Ca_{1/3}MnO_3$ thin film at different temperatures ($T = 294, 50, 16$ K)

Besides ns-order response, a good linear relationship between U_p and E had been observed, and the partial results are shown in Fig. 4, which not only verify the equation $U_p = A_p E$ over a wide range of temperatures and wavelengths, but also allow us to design a peak-voltage-type laser energy meter. To calculate the value of A_p, the measured value should be multiplied by η. Figure 5 depicts the wavelength and temperature dependence of A_p, which shows that the $La_{2/3}Ca_{1/3}MnO_3$ thin-film laser energy meter has spec-

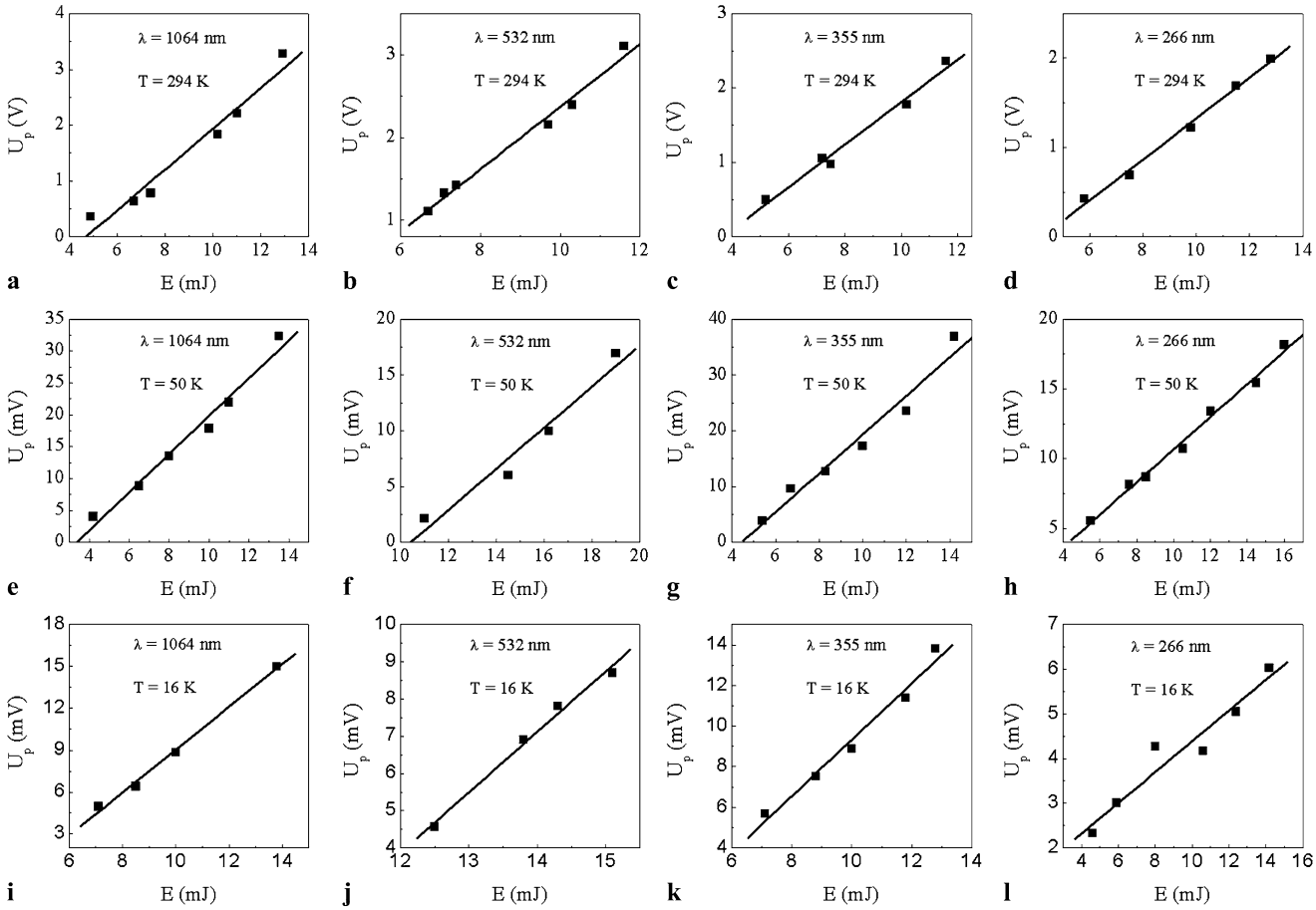

Fig. 4 The linear relationship between the peak voltage U_p of the generated signal and the laser energy per pulse E for the four wavelengths ($\lambda = 1064, 532, 355, 266$ nm) at different temperatures ($T = 294, 50, 16$ K). *Square symbols* represent experimental data, and the solid lines represent the best linear fitting

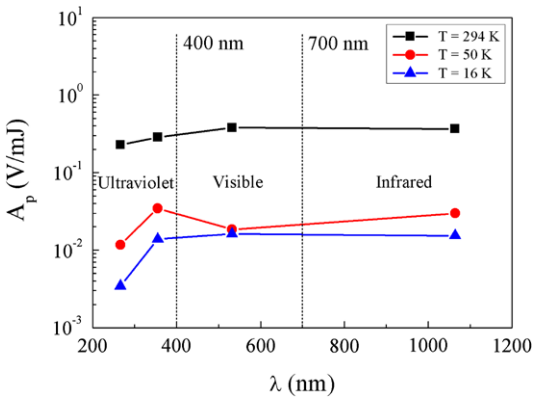

Fig. 5 Wavelength dependence of the sensitivity of the $La_{2/3}Ca_{1/3}MnO_3$ thin film at different temperatures ($T = 294, 50, 16$ K)

trally broad and flat response over a wide range of temperatures from RT to 16 K. A_p has a slight variation with wavelength, which is mainly due to two factors. One is the laser absorption coefficient depending on wavelength. To improve the uniformity of laser absorption, some nanotechnologies can be employed, such as some nanostructures fabricated on the film surface [47–49]. The other is the hot-carrier effect, which makes A_p decrease in UV region because the hot carriers can lead to an energy loss of the laser. Furthermore, Fig. 5 depicts that, at each wavelength, A_p decreases with temperature. Since $S_{ab} - S_c$ and c_0 depend on temperature, Eq. (3) can be written as $A_p \propto (S_{ab} - S_c)/c_0$. Therefore, for the $La_{2/3}Ca_{1/3}MnO_3$ thin film, $(S_{ab} - S_c)/c_0$ decreases with temperature. To obtain better temperature performance, the SCE thin films with nearly temperature-independent $(S_{ab} - S_c)/c_0$ can be selected.

In addition to temperature, different substrates also influence the properties of SCE thin films due to the strain effect. On the one hand, it can influence the T_c of an HTS thin film, e.g., T_c can be 85 and 55 K for the $Bi_2Sr_2CaCu_2O_{8+\sigma}$ thin films grown on an $NdSrAlO_4$ and a $LaSrAlO_4$ substrate, respectively [50]. Consequently, substrate can be used to adjust the operating temperature range of an HTS thin-film laser detector. On the other hand, it was observed that the LITV signals in $La_{2/3}Ca_{1/3}MnO_3$ thin film can be enhanced

by the compress strain introduced by $LaAlO_3$, rather than by the tensile strain introduced by $SrTiO_3$. Therefore, $LaAlO_3$ substrate is more preferable for LCMO thin-film laser detectors [51].

The peak-voltage-type $La_{2/3}Ca_{1/3}MnO_3$ thin-film laser energy meter reported here possesses great advantages over other conventional devices. Firstly, it has ns-order response and spectrally broad (from IR to UV) and flat response. It is known for the semiconductor detectors, though they have ns- or ps-order response, that they suffer the narrow band and nonuniform spectral response due to quantum effect. While for common thermal detectors, although they have spectrally broad response, their response is usually ms-order since a thermal equilibrium process is required. Secondly, it operates over a wide range of temperatures from RT to 16 K. While the bolometers based on SCE thin films only perform well near T_c, most commercial laser energy meters only operate at RT. Thirdly, it is based on anisotropic Seebeck effect and can generate thermoelectric voltage signals; therefore, it is an energy-saving device; in contrast, most bolomers need a constant bias current to sense the resistance change. Fourthly, it can measure both DC and AC signals, while the pyroelectric detectors can only response to AC signals [6, 40, 52]. At last, it can perform in situ real-time measurements.

5 Conclusions

A high-performance peak-voltage-type $La_{2/3}Ca_{1/3}MnO_3$ thin-film laser energy meter has been developed based on the anisotropic Seebeck effect. The device has great advantages over other conventional detectors, such as ns-order response and spectrally broadband (from IR to UV) and flat response over a wide range of temperatures from RT to 16 K, in situ real-time measurement and energy savings, and can be a useful replacement for the commercial pyroelectric power/energy meter. To sum up, by taking the representative $La_{2/3}Ca_{1/3}MnO_3$ thin film as an example, we have presented the great potential of SCE systems for developing next-generation laser detectors and laser energy meters based on the anisotropic Seebeck effect.

Acknowledgements This work was supported by China Postdoctoral Science Foundation (Grant No. 20070410218), the Postdoctoral Foundation of University of Science and Technology of China, the National Natural Science Foundation of China (Grant No. 10274026), and the Natural Science Foundation of Yunnan Province of China (Grant No. 1999E0003Z).

References

1. G.Y. Zhang, P.X. Zhang, H.-U. Habermeier, in *Handbook of Interferometers; Research, Technology and Applications*, ed. by D. Halsey, W. Raynor (Nova Science, New York, 2009)
2. W.H. Huang, X. Li, G.Y. Zhang, in *Handbook of Optical Metrology: Principles and Applications, PART II: Fundamentals of Principles and Techniques for Metrology*, ed. by T. Yoshizawa (Taylor & Francis, CRC Press, London, 2009), Chap. 14, p. 351
3. E. Dagotto, Science **309**, 257 (2005)
4. N. Nagaosa, Science **275**, 1078 (1997)
5. A.J. Millis, Nature **392**, 147 (1998)
6. H. Lengfellner, S. Zeuner, W. Prettl, K.F. Renk, Europhys. Lett. **25**, 375 (1994)
7. S. Zeuner, W. Prettl, H. Lengfellner, Appl. Phys. Lett. **66**, 1833 (1995)
8. P.X. Zhang, G.Y. Zhang, C.T. Lin, H.-U. Habermeier, Egypt. J. Solids **27**, 1 (2004)
9. H. Lengfellner, G. Kremb, A. Schnellbögl, J. Betz, K.F. Renk, W. Prettl, Appl. Phys. Lett. **60**, 501 (1992)
10. K.F. Renk, J. Betz, S. Zeuner, H. Lengfellner, W. Prettl, Physica C **235–240**, 37 (1994)
11. T. Roch, S. Yaghoubzadeh, F.S. Razavi, B. Leibold, R. Praus, H.-U. Habermeier, Appl. Phys. A **67**, 723 (1998)
12. R. Bathe, K.P. Adhi, S.I. Patil, G. Marest, B. Hannoyer, S.B. Ogale, Appl. Phys. Lett. **76**, 2104 (2000)
13. H.-U. Habermeier, X.H. Li, P.X. Zhang, B. Leibold, Solid State Commun. **110**, 473 (1999)
14. X.H. Li, H.-U. Habermeier, P.X. Zhang, J. Magn. Magn. Mater. **211**, 232 (2000)
15. C.L. Chang, A. Kleinhammes, W.G. Moulton, L.R. Testardi, Phys. Rev. B **41**, 11564 (1990)
16. P.X. Zhang, X.M. Wen, M.M. Gu, G.Y. Zhang, Chin. J. Lasers **29**, 205 (2002)
17. P.X. Zhang, C. Wang, G.Y. Zhang, L. Yu, W.K. Lee, H.-U. Habermeier, Opt. Laser Technol. **36**, 341 (2004)
18. H.J. Coufal, R.K. Grygier, J. Opt. Soc. Am. B **6**, 2013 (1989)
19. H.J. Coufal, R.K. Grygier, D.E. Horne, J.E. Fromm, J. Vac. Sci. Technol. A **5**, 2875 (1987)
20. H. Coufal, W. Lee, Appl. Phys. B **44**, 141 (1987)
21. H. Coufal, IEEE Trans. Electr. Insul. **EI-21**, 495 (1986)
22. F. Träger, H. Coufal, T.J. Chuang, Phys. Rev. Lett. **49**, 1720 (1982)
23. B. Sadoulet, AIP Conf. Proc. **1185**, 785 (2009)
24. G.C. Hilton, AIP Conf. Proc. **1185**, 3 (2009)
25. A. Giuliani, Physica B **280**, 501 (2000)
26. D. Twerenbold, Rep. Prog. Phys. **59**, 349 (1996)
27. N. Booth, B. Cabrera, E. Fiorini, Annu. Rev. Nucl. Part. Sci. **46**, 471 (1996)
28. C. Enss, D. McCammon, J. Low Temp. Phys. **151**, 5 (2008)
29. B. Cabrera, J. Low Temp. Phys. **151**, 82 (2008)
30. J.A. Formaggio, E. Figueroa-Feliciano, A.J. Anderson, Phys. Rev. D **85**, 013009 (2012)
31. J. Yan, M.-H. Kim, J.A. Elle, A.B. Sushkov, G.S. Jenkins, H.M. Milchberg, M.S. Fuhrer, H.D. Drew, Nat. Nanotechnol. **7**, 472 (2012)
32. S. Komiyama, O. Astafiev, V. Antonov, T. Kutsuwa, H. Hirai, Nature **403**, 405 (2000)
33. R.H. Hadfield, Nat. Photonics **3**, 696 (2009)
34. J. Wei, D. Olaya, B.S. Karasik, S.V. Pereverzev, A.V. Sergeev, M.E. Gershenson, Nat. Nanotechnol. **3**, 496 (2008)
35. A. Rogalski, Infrared Phys. Technol. **43**, 187 (2002)
36. T.D. Ladd, F. Jelezko, R. Laflamme, Y. Nakamura, C. Monroe, J.L. O'Brien, Nature **464**, 45 (2010)
37. X.-S. Ma, T. Herbst, T. Scheidl, D. Wang, S. Kropatschek, W. Naylor, B. Wittmann, A. Mech, J. Kofler, E. Anisimova, V. Makarov, T. Jennewein, R. Ursin, A. Zeilinger, Nature **489**, 269 (2012)
38. Z. Merali, Nature **492**, 22 (2012)
39. J.-W. Pan, Z.-B. Chen, C.-Y. Lu, H. Weinfurter, A. Zeilinger, M. Zukowski, Rev. Mod. Phys. **84**, 777 (2012)
40. G.Y. Zhang, H.R. Zheng, X.Y. Zhang, D.L. Gao, P.X. Zhang, H.U. Habermeier, Appl. Phys. B **108**, 649 (2012)

41. P.X. Zhang, W.K. Lee, G.Y. Zhang, Appl. Phys. Lett. **81**, 4026 (2002)
42. Th. Zahner, R. Stierstorfer, S. Reindl, T. Schauer, A. Penzkofer, H. Lengfellner, Physica C **313**, 37 (1999)
43. A.J. Nozik, Physica E **14**, 115 (2002)
44. G. Conibeer, Mater. Today **10**, 42 (2007)
45. H. Fujishiro, M. Ikebe, T. Akashi, T. Goto, Physica B **316–317**, 261 (2002)
46. J. Liebe, E. Kraus, L. Haupt, P. Mandal, K. Bärner, Appl. Phys. Lett. **68**, 2343 (1996)
47. W. Lang, K. Kühl, H. Sandmaier, Sens. Actuators A **34**, 243 (1992)
48. S.B. Rim, S. Zhao, S.R. Scully, M.D. McGehee, P. Peumans, Appl. Phys. Lett. **91**, 243501 (2007)
49. J. Zhao, A. Wang, P. Altermatt, M.A. Green, Appl. Phys. Lett. **66**, 3636 (1995)
50. A.H. Li, M. Ionescu, X.L. Wang, S.X. Dou, H. Wang, J. Alloys Compd. **333**, 179 (2002)
51. P.X. Zhang, J.B. Wang, G.Y. Zhang, H.-U. Habermeier, W.K. Lee, Physica C **364–365**, 656 (2001)
52. H.S. Kwok, J.P. Zheng, Phys. Rev. B **46**, 3692 (1992)